

# Electron diffraction from cylindrical nanotubes

L. C. Qin

Department of Materials Science and Engineering, Massachusetts Institute of Technology, Cambridge, Massachusetts 02139

(Received 14 January 1994; accepted 26 April 1994)

Electron diffraction intensities from cylindrical objects can be conveniently analyzed using Bessel functions. Analytic formulas and geometry of the diffraction patterns from cylindrical carbon nanotubes are presented in general forms in terms of structural parameters, such as the pitch angle and the radius of a tubule. As an example the Fraunhofer diffraction pattern from a graphitic tubule of structure [18, 2] has been simulated to illustrate the characteristics of such diffraction patterns. The validity of the projection approximation is also discussed.

## I. INTRODUCTION

The recent experimental advance in the making of carbon nanotubes<sup>1</sup> in laboratories has been most interesting in materials science<sup>2</sup> because of their specific physical properties, such as high-strength mechanical properties,<sup>3</sup> sensitive electronic properties,<sup>4</sup> etc. All these physical properties are very sensitive to the atomic structures. Though it has been known that the tubes are made of graphene sheets, they can still have various geometries in the form of spiral tubes. As a consequence, for instance, the atomic structure of the caps in a closed tubule is directly related to the spiral geometry.<sup>5</sup>

Due to the very small size of the nanotubes, an electron probe offers a unique tool in characterizing the atomic structures in diffraction experiments. It is so partly because fast electrons (10 keV to 1 MeV in energy) have very small wavelengths and partly because the interaction between the incident electrons with the scattering atoms is much stronger compared to other radiations, such as x-rays or neutrons.

Though high-resolution electron microscopy can provide information on the size (radii of the tubes), it is difficult to obtain any structural information along the axial direction, which has been shown both by experimental micrographs<sup>1</sup> and numerical simulations,<sup>6</sup> such as the periodicity, pitch length, pitch angles, etc. On the other hand, electron diffraction patterns contain a great deal of structural information, which sometimes is more easily accessible than in the case of images which are more sensitive to the imaging parameters of the microscope.

Most recently Iijima and Ichihashi<sup>7</sup> have reported structural characterizations of single-shell carbon nanotubes of about 1 nm in diameter using high-resolution electron microscopy and electron diffraction. The geom-

etry of the electron diffraction patterns from the carbon nanotubes was also discussed in Ref. 8 using constructed reciprocal spaces of the tubules.

In the present paper electron diffraction patterns from such nanotubes are analyzed. Analytic expressions for the diffraction intensities are given. The geometry of diffraction patterns is also discussed in terms of structural parameters of the nanotubes. As an example, the characteristics of the diffraction pattern from a single layer graphitic tubule of diameter 1.33 nm are presented to illustrate the results.

## II. DIFFRACTION FROM CYLINDRICAL OBJECTS

In electron diffraction the reflection intensity  $I(\mathbf{q})$  is equal to the square of the absolute value of the corresponding structure factor  $F(\mathbf{q})$ , which is defined as

$$F(\mathbf{q}) = \sum_j f_j \exp(2\pi i \mathbf{q} \cdot \mathbf{r}_j), \quad (1)$$

where  $f_j$  is the atomic scattering amplitudes,  $\mathbf{r}_j$  is the atomic coordinates, and  $\mathbf{q}$  is the scattering vector

$$\mathbf{q} = \frac{2 \sin(\Theta/2)}{\lambda}, \quad (2)$$

in which  $\Theta$  and  $\lambda$  are the scattering angle and the electron wavelength, respectively. It is also proportional to the Fourier transform of the Coulombic potential function of the scattering object  $V(\mathbf{r})$

$$F(\mathbf{q}) = \int V(\mathbf{r}) \exp(2\pi i \mathbf{q} \cdot \mathbf{r}) d\mathbf{r}. \quad (3)$$

For a cylindrical object which is periodic in its axial direction  $z$ , the structure factor  $F(R, \Phi, l)$  can be conveniently expressed in cylindrical coordinates  $(r, \phi, z)$

(see Appendix) as

$$F(R, \Phi, l) = \frac{1}{c} \sum_{n=-\infty}^{+\infty} \exp\left[in\left(\Phi + \frac{\pi}{2}\right)\right] \times \int_0^c \int_0^{2\pi} \int_0^\infty V(r, \phi, z) J_n(2\pi Rr) \times \exp\left[-i\left(n\phi + \frac{2\pi lz}{c}\right)\right] r dr d\phi dz, \quad (4)$$

where  $J_n$  is the Bessel function of order  $n$ ,  $c$  is the periodicity of the object along the  $z$ -direction, and  $(R, \Phi, Z)$  are the cylindrical coordinates in the corresponding reciprocal space.

The scattering amplitude from a continuous spiral line of radius  $r_0$  and periodicity  $C$ , i.e.,

$$V(r, \phi, z) = V_0 \delta(r - r_0) \delta\left(\phi + \frac{2\pi z}{C}\right), \quad (5)$$

is therefore

$$F_c(R, \Phi, l) = r_0 V_0 J_l(2\pi r_0 R) \exp\left[i\left(\Phi + \frac{\pi}{2}\right)l\right], \quad (6)$$

and the corresponding diffraction intensity distribution  $I_c(R, \Phi, l)$  is

$$I_c(R, \Phi, l) = |F_c(R, \Phi, l)|^2 = r_0^2 V_0^2 [J_l(2\pi r_0 R)]^2. \quad (7)$$

For a structure composed of discrete atoms located on a helical line, which has a periodicity of  $c$  with  $q$  turns and  $p$  points, as schematically illustrated in Fig. 1, the structure can be expressed as the product of the continuous spiral and a set of planes located at  $z = j\Delta$ , where  $j$  is an integer. In Fourier space, the nonextinction layers are therefore the convolution of the structure factor of a continuous spiral with the Fourier transform of this set of planes, which is a set of discrete points located at  $Z = j/\Delta$  on the  $Z$ -axis:

$$Z = \frac{l}{c} = \frac{n}{C} + \frac{m}{\Delta}, \quad (8)$$

where  $m$  is an integer and  $n$  determines the order of Bessel functions due to the continuous spiral. The structure factor is, hence,

$$F(R, \Phi, l) = \sum_{n=-\infty}^{+\infty} J_n(2\pi r_0 R) \times \exp\left[in\left(\Phi + \frac{\pi}{2}\right)\right], \quad (9)$$

where  $l$  and  $n$  are related by the selection rule:

$$l = nq + mp, \quad (10)$$

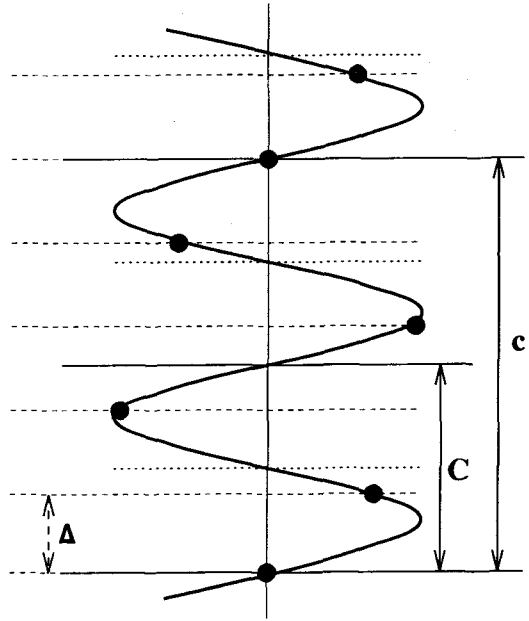


FIG. 1. Schematic structure of a discontinuous spiral. Lattice points are located at a continuous spiral with equal spacing along the  $z$ -axis.

where

$$p = \frac{c}{\Delta} \quad (11)$$

and

$$q = \frac{c}{C}. \quad (12)$$

When there is  $N$ -fold rotational symmetry along the  $z$ -axis, then we have

$$F(R, \Phi, l) = \sum_{k=-\infty}^{+\infty} J_{kN}(2\pi r_0 R) \exp\left[ikN\left(\Phi + \frac{\pi}{2}\right)\right] = \sum_{n=-\infty}^{+\infty} J_n(2\pi r_0 R) \exp\left[in\left(\Phi + \frac{\pi}{2}\right)\right], \quad (13)$$

and the selection rule

$$l = nq + mp \quad (14)$$

is subject to the following constraint on the values of  $n$ :

$$n = 0, \pm N, \pm 2N, \pm 3N \dots \quad (15)$$

If there is more than one atom per unit cell (asymmetric unit), a summation should be done over all the atoms within the unit cell:

$$F(R, \Phi, l) = \sum_{n=-\infty}^{+\infty} \exp\left[in\left(\Phi + \frac{\pi}{2}\right)\right] \times \sum_j f_j J_n(2\pi r_j R) \times \exp\left[i\left(n\phi_j + \frac{2\pi lz_j}{c}\right)\right], \quad (16)$$

where the summation over  $j$  is done over all atoms in an asymmetric unit cell. For the case where all atoms are located on a cylindrical surface of radius  $r_0$ , we have

$$F(R, \Phi, l) = \sum_{n=-\infty}^{+\infty} \exp\left[in\left(\Phi + \frac{\pi}{2}\right)\right] \times J_n(2\pi r_0 R) \sum_j f_j \times \exp\left[i\left(n\phi_j + \frac{2\pi lz_j}{c}\right)\right]. \quad (17)$$

We can also use the radial projection method<sup>9</sup> to calculate the structure factors. In the radial projection plane, the coordinates are related to the cylindrical coordinates by

$$\begin{cases} x_j = r_0 \phi_j \\ z_j = z_j \end{cases} \quad (18)$$

and the structure factor  $T_{nl}$  which describes the scattering amplitude from the radially projected structure is

$$T_{nl} = \sum_j f_j \exp\left[2\pi i\left(\frac{nx_j}{a} + \frac{lz_j}{c}\right)\right], \quad (19)$$

where

$$a = 2\pi r_0. \quad (20)$$

Substituting Eq. (18) into Eq. (17), we obtain the total structure factor in terms of the coordinates in the radial projection net:

$$F(R, \Phi, l) = \sum_{n=-\infty}^{+\infty} \exp\left[in\left(\Phi + \frac{\pi}{2}\right)\right] J_n(2\pi r_0 R) \times \sum_j f_j \exp\left[2\pi i\left(\frac{nx_j}{a} + \frac{lz_j}{c}\right)\right] = \sum_{n=-\infty}^{+\infty} B_n(R, \Phi) T_{nl}; \quad (21)$$

where

$$B_n(R, \Phi) = \sum_{n=-\infty}^{+\infty} \exp\left[in\left(\Phi + \frac{\pi}{2}\right)\right] J_n(2\pi r_0 R), \quad (22)$$

where the summation is done over all atoms in a unit cell representing a lattice point in the radial projection net. The indices  $n$  and  $l$  follow the same selection rule given by Eq. (10).

### III. STRUCTURE OF NANOTUBES

The lattice structure of a single-shell nanotube of radius  $r_0$  can be characterized by two integers  $[u, v]$  in the hexagonal lattice plane.<sup>10</sup> Figure 2 gives such a graphitic sheet with half of the radial projection for a  $[18, 2]$  tubule marked. The rectangular has two sides. One is the circumference of the tubule  $a = 2\pi r_0$ , and the other is the periodicity  $c$  along  $z$ -direction:

$$\begin{aligned} \mathbf{a} &= [u_1, v_1] \\ &= u_1 \mathbf{a}_1 + v_1 \mathbf{a}_2 \end{aligned} \quad (23)$$

where  $\mathbf{a}_1$  and  $\mathbf{a}_2$  are the basis vectors of the hexagonal graphite lattice with

$$\begin{cases} a_1 = a_2 = a_0 \\ \mathbf{a}_1 \cdot \mathbf{a}_2 = -1/2 \end{cases} \quad (24)$$

and  $\mathbf{c} = [u_2, v_2]$  is perpendicular to  $\mathbf{a}$ , which can be determined by

$$(u_1 \mathbf{a}_1 + v_1 \mathbf{a}_2) \cdot (u_2 \mathbf{a}_1 + v_2 \mathbf{a}_2) = 0, \quad (25)$$

or

$$\frac{u_2}{v_2} = \frac{u_1 - 2v_1}{2u_1 - v_1}. \quad (26)$$

The helical angle  $\alpha$  is given by

$$\cos \alpha = \frac{2u_1 - v_1}{2(u_1^2 + v_1^2 - u_1 v_1)^{1/2}}. \quad (27)$$

When the unit cell of the hexagonal graphene is used as an asymmetric unit, the number of basic helices  $N$  is equal to the value of  $v_1$ . Though multiple helices can be incorporated into a single basic helix, often it is more convenient to have the basic helix as composed of single carbon hexagons. In fact, multiple helices will introduce  $N$ -fold rotational symmetry about the  $z$ -axis.

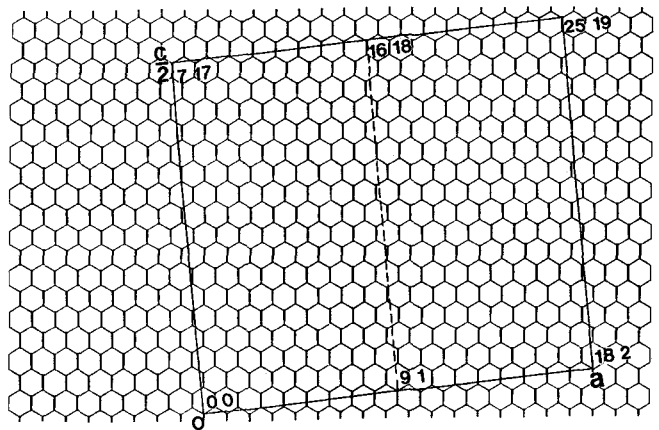


FIG. 2. A single graphene sheet shows a half unit cell of the  $[18, 2]$  tubule in radial projection.

The number of turns  $q$  is given by

$$\begin{aligned}
 q &= \frac{c}{C} \\
 &= \frac{c}{a \tan \alpha} \\
 &= \frac{(2u_1 - v_1)(u_2^2 + v_2^2 - u_2v_2)^{1/2}}{v_1[3(u_1^2 + v_1^2 - u_1v_1)]^{1/2}}, \quad (28)
 \end{aligned}$$

and

$$\begin{aligned}
 p &= \frac{c}{\Delta} \\
 &= \frac{qa}{a_0 \cos \alpha} \\
 &= \frac{u_1^2 + v_1^2 - u_1v_1}{2u_1 - v_1} q \quad (29)
 \end{aligned}$$

is the number of lattice points on a basic helix.

Since the radial projection of carbon nanotubes is just a graphitic sheet, in calculating the structure factors or diffraction intensities Eq. (21) will be the most convenient one. There are two carbon atoms in the asymmetric unit with coordinates  $(0, 0)$  and  $(1/3, 2/3)$  in units of  $a_0 = 0.2451$  nm. The fraction coordinates are therefore

$$\begin{aligned}
 x_1 &= 0 \\
 z_1 &= 0 \quad (30)
 \end{aligned}$$

and

$$\begin{aligned}
 x_2 &= \frac{1}{3(u_1^2 + v_1^2 - u_1v_1)^{1/2}} \\
 z_2 &= \frac{2}{3(u_2^2 + v_2^2 - u_2v_2)^{1/2}}. \quad (31)
 \end{aligned}$$

The corresponding cylindrical coordinates are

$$\begin{aligned}
 \phi_j &= \frac{2\pi qj}{p} \\
 z_j &= x_j \tan \alpha. \quad (32)
 \end{aligned}$$

#### IV. AN EXAMPLE

As an example, for the graphitic tubule (Fig. 3) indexed by  $\mathbf{a} = [18, 2]$ , we can obtain  $\mathbf{c} = [14, 34]$ , and

$$a = 4.19 \text{ nm} \quad \text{or} \quad d = 2r_0 = 1.33 \text{ nm} \quad (33)$$

$$c = 7.25 \text{ nm}. \quad (34)$$

There are two basic helices, i.e.,

$$N = 2, \quad (35)$$

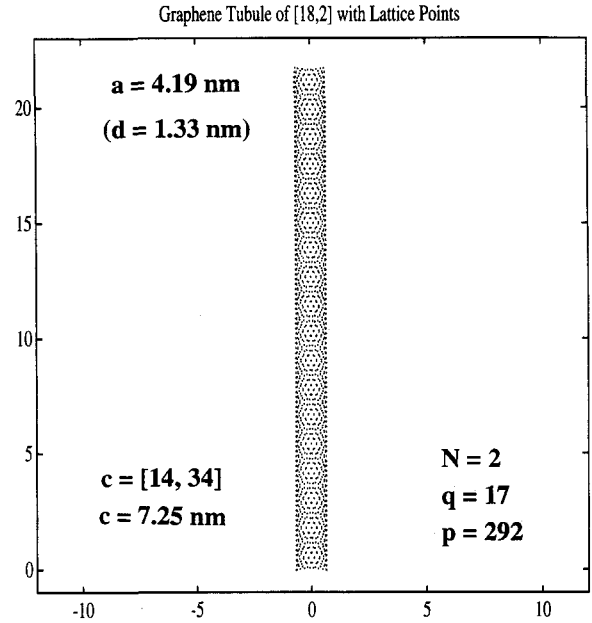


FIG. 3. Projection of the  $[18, 2]$  graphene tubule of diameter  $d = 1.33$  nm. The units of both horizontal and vertical axes are nm.

and other parameters are

$$q = 17 \quad (36)$$

$$p = 292 \quad (37)$$

$$\alpha = 5.8^\circ \quad (38)$$

$$\Delta = 0.0248 \text{ nm} \quad (39)$$

$$C = 0.426 \text{ nm}. \quad (40)$$

The selection rule is

$$\begin{aligned}
 l &= nq + mp \\
 &= 17n + 292m \quad (41)
 \end{aligned}$$

with  $n$  taking values of multiples of  $N$ :

$$n = 0, \pm 2, \pm 4, \pm 6, \dots \quad (42)$$

The following table lists some values for  $l$ ,  $n$ , and  $m$ :

$l = 0,$	$n = 0,$	$m = 0$
$l = 2,$	$n = 86,$	$m = -5$
$l = 4,$	$n = -120,$	$m = 7$
$l = 6,$	$n = -34,$	$m = 2$
$l = 8,$	$n = 52,$	$m = -3$
$l = 10,$	$n = 138,$	$m = -8$
$l = 12,$	$n = 68,$	$m = 4$
$\cdot$	$\cdot$	$\cdot$
$\cdot$	$\cdot$	$\cdot$
$\cdot$	$\cdot$	$\cdot$
$l = 34,$	$n = 2,$	$m = 0$
$l = 68,$	$n = 4,$	$m = 0$
$l = 102,$	$n = 6,$	$m = 0$

Since the value of Bessel functions decreases very rapidly with increasing values of their order, only the terms with small  $n$  are significant. Therefore, the layer lines of indices of multiples of 34 are of relatively high intensities. For the above example, the first two layer lines are located at

$$34c^* = \frac{1.15}{a_0} = 4.65 \text{ nm}^{-1} \quad (43)$$

and

$$68c^* = \frac{2.30}{a_0} = 9.30 \text{ nm}^{-1}. \quad (44)$$

The first maxima of Bessel functions  $J_2(u)$  and  $J_4(u)$  occur at  $u_2 = 3.05$  and  $u_4 = 5.30$ , respectively, where  $u = 2\pi r_0 R$ . If we use the diameter of the tubule as  $2r_0 = 1.33 \text{ nm}$ , then we have the corresponding values for  $R$  at the above maxima:

$$R_2 = 0.73 \text{ nm}^{-1} \quad (45)$$

and

$$R_4 = 1.27 \text{ nm}^{-1}. \quad (46)$$

With the numbers obtained above, we can calculate the angle between the maximum intensity rows from such a tubule:

$$\begin{aligned} \theta &\approx 2 \tan^{-1} \left( \frac{R_2}{34c^*} \right) \\ &\approx 2 \tan^{-1} \left( \frac{R_4}{68c^*} \right) \\ &\approx 18^\circ. \end{aligned} \quad (47)$$

Consequently, the value of  $\theta$  can be used to identify the atomic pitch angle of the tubule.

Depicted in Fig. 4 is the diffraction intensity distribution from a [18,2] tubule with layer lines indexed in accordance with the selection rule.

Shown in Fig. 5 is the power spectrum of Fig. 3, which gives the geometric characteristics as discussed in the analytic expressions. The strong noise background is due to the relatively small number of scattering points, as can also be seen from the experimental electron diffraction patterns.<sup>7,8</sup>

## V. DISCUSSION

It should be noticed that for the above example, only even values of  $l$  appeared in the nonextinction layer lines. It is because of the change in the periodicity  $c$ , which has changed to half of the original value for the above example due to the 2-fold symmetry. This introduces the systematic extinction, like the case in crystal diffraction with nonprimitive lattices. In general, when there is an  $N$ -fold axis, the rule for systematic extinction is

$$l \neq kN, \quad (48)$$

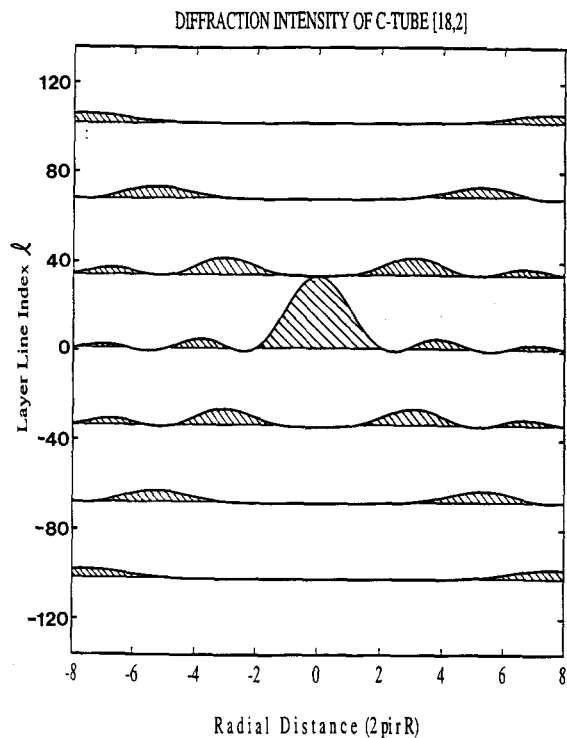


FIG. 4. Fraunhofer diffraction intensity distribution from a [18,2] tubule. Layer lines were indexed according to relevant selection rules.

where  $k$  is an integer. However, this applies to only the layer lines with  $m = 0$ , which is often the only ones of observable intensities.

It is interesting to note that the length of the basis vector of the reciprocal lattice of the two-dimensional

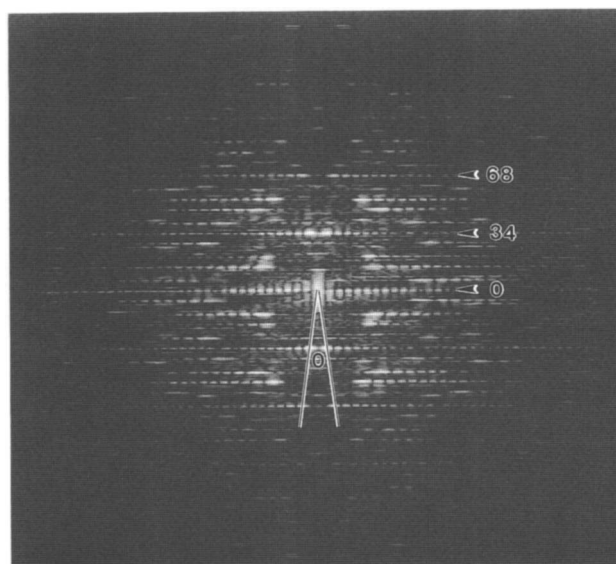


FIG. 5. Power spectrum of the [18,2] tubule shown in Fig. 2. The first strong layer line is  $34/c$ , and the angle between the Bessel peaks is about  $18^\circ$ .

graphitic lattice is

$$a_0^* = \frac{1}{a_0 \cos(\pi/6)} = \frac{1.15}{a_0} = 4.65 \text{ nm}^{-1}, \quad (49)$$

which is equal to the value of  $34c^*$  [Eq. (43)] where the first layer line appears. This has often led to a trend to index the diffraction patterns from a graphitic tubule using the indices of the hexagonal lattice of a graphene.

Since the wavelength of fast electrons (e.g.,  $3.7 \times 10^{-3}$  nm at 100 kV and  $2.5 \times 10^{-3}$  nm at 200 kV, respectively) is very small, the projection approximation of electron diffraction theory is good for most cases when the scattering objects are composed of carbons in the form of graphitic tubules. However, when the radii of the tubules are also very small, the projected structure may deviate substantially from the projection of graphitic sheets. In such cases, the cylindrical curvature cannot be ignored in the projected structure, as evidenced by Fig. 3, which deviates largely from the projected structure of graphitic sheet, as shown in Fig. 2. Consequently, the diffraction patterns are much more strongly affected by the cylindrical geometry, as can be seen from the diffraction intensity distributions. Only when the radii of the tubules are much larger, the geometry of the diffraction patterns may be well approximated as the overlapping of two flat graphitic sheets rotated by  $2\alpha$  with respect to each other.

## VI. CONCLUSIONS

Analytic expressions for the electron diffraction intensities and geometry from spiral graphene tubules have been given to help characterize the structure of the carbon nanotubes in transmission electron microscopes. The diffraction intensity distribution is described by Bessel functions, and the atomic structure can be deduced by examining the experimental diffraction patterns.

## ACKNOWLEDGMENTS

The research was supported by Department of Energy Grant DE-FG02-89ER45396 supervised by Professor L. W. Hobbs, whose encouragement is also gratefully acknowledged.

## REFERENCES

1. S. Iijima, *Nature* **354**, 56 (1991).
2. M. S. Dresselhaus, G. Dresselhaus, and P. C. Eklund, *J. Mater. Res.* **8**, 2054 (1993).
3. D. H. Robertson, D. W. Brenner, and J. W. Mintmire, *Phys. Rev. B* **45**, 12592 (1992).
4. R. Saito, M. Fujita, G. Dresselhaus, and M. S. Dresselhaus, *Phys. Rev. B* **46**, 1804 (1992).
5. M. S. Dresselhaus, G. Dresselhaus, and R. Saito, *Phys. Rev. B* **45**, 6234 (1992).
6. L. C. Qin, unpublished.
7. S. Iijima and T. Ichihashi, *Nature* **363**, 603 (1993).
8. X. F. Zhang, X. B. Zhang, G. van Tendeloo, S. Amelinckx, M. Op de Beeck, and J. Van Landuyt, *J. Cryst. Growth* **130**, 368 (1993).
9. A. Klug, F. H. C. Crick, and H. W. Wyckoff, *Acta Crystallogr.* **11**, 199 (1958).
10. N. Hamada, S. Sawada, and A. Oshiyama, *Phys. Rev. Lett.* **68**, 1579 (1992).

## APPENDIX

In a cylindrical coordinate system, the coordinates  $(r, \phi, z)$  are related to the Cartesian coordinates  $(x, y, z)$  by the following transformation:

$$\begin{cases} x = r \cos \phi \\ y = r \sin \phi \\ z = z, \end{cases} \quad (50)$$

or for the coordinates in reciprocal space

$$\begin{cases} X = R \cos \Phi \\ Y = R \sin \Phi \\ Z = Z. \end{cases} \quad (51)$$

The structure factor in the cylindrical coordinate system then becomes

$$\begin{aligned} F(R, \Phi, Z) &= \int V(\mathbf{r}) \exp(2\pi i \mathbf{q} \cdot \mathbf{r}) d\mathbf{r} \\ &= \int_{-\infty}^{+\infty} \int_0^{2\pi} \int_0^{\infty} V(r, \phi, z) \\ &\quad \times \exp\{2\pi i[rR \cos(\phi - \Phi) + zZ]\} \\ &\quad \times r dr d\phi dz. \end{aligned} \quad (52)$$

This is a general expression for any object geometry in a cylindrical coordinate system.

Expanding the potential function  $V(r, \phi, z)$  into Fourier series

$$V(r, \phi, z) = \sum_{n=-\infty}^{+\infty} V_n(r, z) \exp(in\phi), \quad (53)$$

and substitute it into Eq. (52):

$$\begin{aligned} F(R, \Phi, Z) &= \int_{-\infty}^{+\infty} \int_0^{2\pi} \int_0^{\infty} V(r, \phi, z) \\ &\quad \times \exp[2\pi i R r \cos(\phi - \Phi)] \\ &\quad \times \exp(2\pi i z Z) r dr d\phi dz \\ &= \sum_{n=-\infty}^{+\infty} \int_{-\infty}^{+\infty} \int_0^{\infty} V_n(r, z) \exp(in\Phi) \\ &\quad \times \left\{ \int_0^{2\pi} \exp\left[2\pi i r R \cos(\phi - \Phi) \right. \right. \\ &\quad \left. \left. + in(\phi - \Phi)\right] \right. \\ &\quad \left. \times d\phi \right\} \exp(2\pi i z Z) r dr dz \\ &= \sum_{n=-\infty}^{+\infty} \exp\left[in\left(\frac{\pi}{2} + \Phi\right)\right] \end{aligned}$$

$$\begin{aligned} & \times \int_{-\infty}^{+\infty} \int_0^{\infty} V_n(r, z) \exp(2\pi izZ) \\ & \times J_n(2\pi rR) 2\pi r dr dz, \end{aligned} \quad (54)$$

where  $J_n$  is the Bessel function of order  $n$  defined by

$$2\pi i^n J_n(u) = \int_0^{2\pi} \exp(iu \cos \phi + in\phi) d\phi. \quad (55)$$

Noticing

$$V_n(r, z) = \frac{1}{2\pi} \int_0^{2\pi} V(r, \phi, z) \exp(-in\phi) d\phi, \quad (56)$$

we therefore have

$$\begin{aligned} F(R, \Phi, Z) &= \sum_{n=-\infty}^{+\infty} \exp\left[in\left(\frac{\pi}{2} + \Phi\right)\right] \\ & \times \int_{-\infty}^{+\infty} \int_0^{\infty} \left[ \int_0^{2\pi} V(r, \phi, z) \right. \\ & \times \exp(-in\phi) d\phi \left. \right] \exp(2\pi izZ) \\ & \times J_n(2\pi rR) r dr dz \\ &= \sum_{n=-\infty}^{+\infty} \exp\left[in\left(\frac{\pi}{2} + \Phi\right)\right] \\ & \times \int_{-\infty}^{+\infty} \int_0^{2\pi} \int_0^{\infty} V(r, \phi, z) \\ & \times J_n(2\pi Rr) \exp(2\pi izZ) \\ & \times \exp(-in\phi) r dr d\phi dz. \end{aligned} \quad (57)$$

When the object has an  $N$ -fold rotation axis along the  $z$ -direction, i.e.,

$$V(r, \phi, z) = V\left(r, \phi + \frac{2\pi}{N}, z\right), \quad (58)$$

the Fourier expansion is

$$V(r, \phi, z) = \sum_{n=-\infty}^{+\infty} V_{nN}(r, z) \exp(inN\phi) \quad (59)$$

where

$$\begin{aligned} V_{nN}(r, z) &= \frac{N}{2\pi} \int_0^{2\pi/N} V(r, \phi, z) \\ & \times \exp(-inN\phi) d\phi. \end{aligned} \quad (60)$$

The structure factor  $F(R, \Phi, Z)$  can therefore be related to the potential function  $V(r, \phi, z)$  by

$$F(R, \Phi, Z) = \sum_{n=-\infty}^{+\infty} \exp\left[inN\left(\Phi + \frac{\pi}{2}\right)\right]$$

$$\begin{aligned} & \times \int_{-\infty}^{+\infty} \int_0^{\infty} V_{nN}(r, z) \exp(2\pi izZ) \\ & \times J_{nN}(2\pi rR) 2\pi r dr dz \\ &= N \sum_{n=-\infty}^{+\infty} \exp\left[inN\left(\Phi + \frac{\pi}{2}\right)\right] \\ & \times \int_{-\infty}^{+\infty} \int_0^{2\pi/N} \int_0^{\infty} V(r, \phi, z) \\ & \times J_{nN}(2\pi rR) \exp(2\pi izZ) \\ & \times \exp(-inN\phi) r dr d\phi dz. \end{aligned} \quad (61)$$

When the object is periodic in the  $z$ -direction with a periodicity of  $c$ , the Fourier expansion of the potential function is

$$\begin{aligned} V(r, \phi, z) &= \sum_{n=-\infty}^{+\infty} \sum_{l=-\infty}^{+\infty} V_{nl}(r) \\ & \times \exp\left(in\phi + \frac{2\pi ilz}{c}\right), \end{aligned} \quad (62)$$

and we can similarly incorporate the  $z$ -components into the relevant equations:

$$\begin{aligned} F(R, \Phi, l) &= \frac{1}{c} \sum_{n=-\infty}^{+\infty} \exp\left[in\left(\Phi + \frac{\pi}{2}\right)\right] \\ & \times \int_0^c \int_0^{2\pi} \int_0^{\infty} V(r, \phi, z) \\ & \times J_n(2\pi Rr) \\ & \times \exp\left[-i\left(n\phi + \frac{2\pi lz}{c}\right)\right] r dr d\phi dz, \end{aligned} \quad (63)$$

or

$$F(R, \Phi, l) = \sum_{n=-\infty}^{+\infty} F_{nl}(R) \exp(in\Phi) \quad (64)$$

where

$$\begin{aligned} F_{nl}(R) &= \exp\left(in\frac{\pi}{2}\right) \int_0^{\infty} V_{nl}(r) \\ & \times J_n(2\pi Rr) 2\pi r dr, \end{aligned} \quad (65)$$

$$\begin{aligned} V_{nl}(r) &= \frac{1}{2\pi c} \int_0^c \int_0^{2\pi} V(r, \phi, z) \exp(-in\phi) \\ & \times \exp\left(-\frac{2\pi ilz}{c}\right) d\phi dz. \end{aligned} \quad (66)$$